Inorganic Chemistry

Article

Characterization and Properties of Novel Infrared Nonlinear Optical Crystal CsGe(Br$_x$Cl$_{1−x}$)$_3$

Zhi-Guang Lin,*,† Li-Chuan Tang,‡ and Chang-Pin Chou†

Department of Mechanical Engineering, National Chiao Tung University, Hsinchu 305, Taiwan, R.O.C., and Department of Electrical Engineering, Chung-Cheng Institute of Technology, National Defense University, Taoyuan 353, Taiwan, R.O.C

Innovative infrared nonlinear optical crystals CsGe(Br$_x$Cl$_{1−x}$)$_3$ were synthesized. Their powder X-ray diffraction patterns indicated that they had rhombohedral structures with (*R*3*m*, No. 160) space group symmetry. Their structural distortion increased with *x*. The Kurtz powder techniques revealed that the nonlinear optical efficiency of CsGeBr$_3$ is about 9.64 times larger than that of rhombohedral CsGeCl$_3$ and 28.29 times larger than that of KH$_2$PO$_4$ (KDP); most importantly, CsGe(Br$_x$Cl$_{1−x}$)$_3$ is phase-matchable. The transparent infrared spectrum of rhombohedral CsGe(Br$_x$Cl$_{1−x}$)$_3$ was extended to over 30 μm and demonstrated its potential in the field of nonlinear optics and applicability in the infrared region.

1. Introduction

Frequency conversion is an essential technique for extending laser frequency ranges. Nonlinear optical (NLO) crystals are indispensable in applying this approach in an efficient frequency-shifting device. Several useful crystals, such as KH$_2$PO$_4$ (KDP), LiNbO$_3$, KTiOPO$_4$ (KTP), β-BaB$_2$O$_4$ (BBO), and LiB$_3$O$_5$ (LBO),[1] have been discovered and successfully utilized for converting laser frequencies into visible and ultraviolet radiation, but they are not transparent in the mid-infrared region. Lack of material transparency in the mid-infrared region is not the only obstacle. Other factors such as the absence of a center of symmetry and a high optical damage threshold[2] are also problematic. Therefore, alternative materials have been developed. They include compound semiconductors such as GaSe,[3,4] AgGaS$_2$,[5–8] AgGaSe$_2$,[9]

ZnGeP$_2$,[1,10] Tl$_3$AsS$_3$,[11] and Tl$_3$AsSe$_3$.[12] Although these crystals seem to exhibit appropriate nonlinearity, they either are difficult to produce or have low optical damage thresholds,[13–15] since their bandgaps are narrow. Hence, the search for new infrared NLO crystals with excellent properties, especially a high damage threshold, has become a key area of research in NLO material science and laser technology.[1]

Various ternary halides, such as ABX$_3$ (A = Cs; B = Ge; X = Cl, Br, or I),[16–18] have been discovered to exhibit

* Author to whom correspondence should be addressed. Tel: 886-3-5712121-55157. Fax: 886-3-5720634. E-mail: zglin.me91g@nctu.edu.tw.
† National Chiao Tung University.
‡ National Defense University.

(1) Dmitriev, V. G., Gurzadyan G. G., Nikogosyan, D. N. *Handbook of Nonlinear Optical Crystals*; Springer Topics in Optical Sciences, Vol 64; Springer-Verlag: Berlin, 1991.
(2) Auston, D. H.; Hellwarth, R. W.; Kaplan, A. E.; Kelley, P. L.; Leonberger, F. J.; Lytel, R. S.; Majerfeld, A.; Neurgaonkar, R. R.; Peyghambarian, N.; Prasad, P. N.; Rakuljic, G. A.; Shen, Y.-R.; Smith, P. W.; Stamatoff, J.; Stegeman, G. I.; Stillman, G. E.; Tang, C. L.; Temkin, H.; Thakur, M. K.; Valley, G. C.; Wolff, P. A.; Woods, C. L. *Appl. Opt.* **1986**, *26*, 211.
(3) Cenzual, K.; Gelato, L. M.; Penzo, M.; Parthe, E. *Acta Crystallogr.* **1991**, *B47*, 433.
(4) Boyd, L. D.; Buehler, E.; Storz, F. G. *Appl. Phys. Lett.* **1971**, *18*, 301.
(5) Kupecek, P. J.; Schwartz, C. A.; Chemla, D. S. *IEEE J. Quantum Electron.* **1974**, *10*, 540.
(6) Bhar, G. C.; Smith, R. C. *IEEE J. Quantum Electron.* **1974**, *10*, 546.
(7) Jaffe, J. E.; Zunger, A. *Phys. Rev. B* **1984**, *28*, 5822.
(8) Shen, Y. R. *The Principles of Nonlinear Optics*; John Wiley and Sons: New York, 2002.
(9) Komine, H.; Fukumoto, J. M.; Long, W. H.; Stappaerts, E. A. CLEO94 Technical Digest paper CPD, 1994, Vol. 14-1, p 31.
(10) Mason, P. D.; Jackson, D. J.; Gorton, E. K. *Opt. Commun.* **1994**, *110*, 163.
(11) Feichtner, J. D.; Roland, G. W. *Appl. Opt.* **1972**, *11*, 993.
(12) Suhre, D. R. *Appl. Phys. B: Laser Opt.* **1991**, *52*, 367.
(13) Buehler, E.; Wernick, J. H. *J. Cryst. Growth* **1970**, *8*, 324.
(14) Shay, J. L.; Wernick, J. H. *Ternary Chalcopyrite Semiconductor: Growth, Electronic Properties and Applications*; Pergamon Press: Oxford, U.K., 1975.
(15) Yoo, K. C.; Storrick, R. P.; Henningsen, T.; Spitznagel, J. A.; Hopkins, R. H. *J. Cryst. Growth* **1992**, *125*, 208.
(16) Zhang, J.; Su, N.; Yang, C.; Qin, J.; Ye, N.; Wu, B.; Chen, C. *Chem. Proc. SPIE* **1998**, *3556*, 1.
(17) Ewbank, M. D.; Cunningham, F.; Borwick, R.; Rosker, M. J.; Gunter, P. CLEO97 paper, 1997, Paper CFA7, p 462.
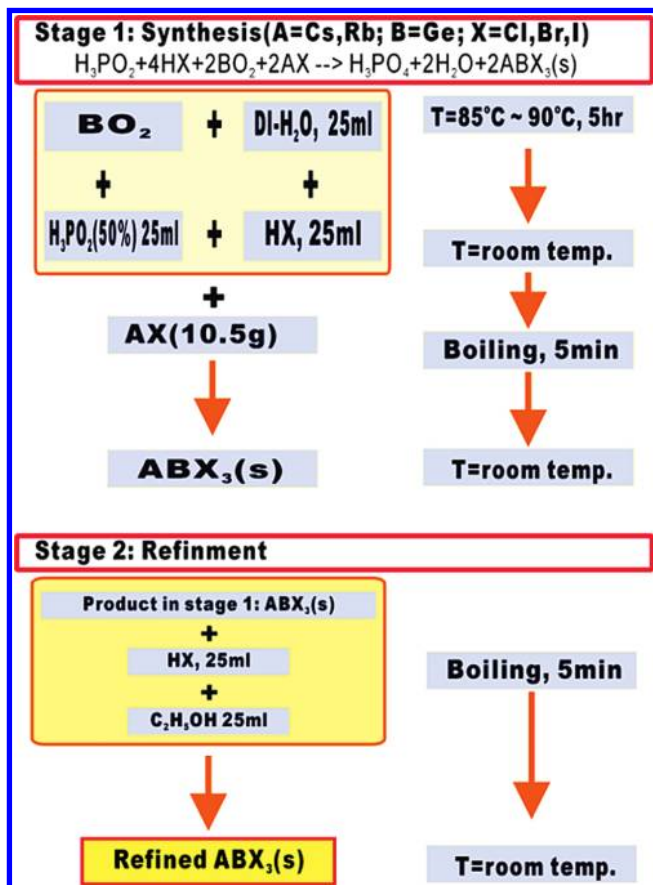(18) Tang, L. C.; Chang, C. S.; Huang, J. Y. *J. Phys.: Condens. Matter* **2000**, *12*, 9129.

Figure 1. The synthesis procedure for rhombohedral nonlinear optical crystals CsGe(Br$_x$Cl$_{1-x}$)$_3$.

Figure 2. EPMA measurements of CsGe(Br$_x$Cl$_{1-x}$)$_3$, $x = 0$, 1/4, 1/2, 3/4, or 1.

Figure 3. The thermal analysis of rhombohedral nonlinear optical crystals of CsGe(Br$_x$Cl$_{1-x}$)$_3$.

Figure 4. X-ray powder diffraction of the NLO crystals CsGe(Br$_x$Cl$_{1-x}$)$_3$. It can be seen that the XRD peaks shift with Br composition.

second-order NLO properties. The damage threshold of CsGeCl$_3$ reaches 200 MW/cm^2.[19] The optical damage threshold and the range of transparency of materials are related to the magnitude of the band gap, while the optical nonlinearity is inversely proportional to the cube of the band gap.[8] The ternary halides recently have been recognized as a new category of nonlinear optical materials, which are potentially applicable to both the visible and the infrared spectra. The linear and NLO properties of CsGe(Br$_x$Cl$_{1-x}$)$_3$ can be adjusted by varying the alloy composition to meet the demand for specific applications. This investigation presents a method for synthesizing crystals and measuring the optical properties of each composition. Nonlinear coefficients of CsGe(Br$_x$Cl$_{1-x}$)$_3$, $x = 0$, 1/4, 1/2, 3/4, and 1 are also set to reveal the potential of these crystals in NLO applications.

2. Experimental Procedures

2.1. Synthesis. Figure 1 presents the synthetic procedure, which was modified from that proposed by Gu et al.[19–21] Chritensen and Tananaev et al.[22,23] used different synthetic methods, but their

methods were complex and offered poor productivity. In this study, H$_3$PO$_2$ (50%) was loaded with HBr (48%), HCl (37%) and GeO$_2$ (99.999%) into a 250 mL beaker and then heated to 95 °C. The solution was vigorously mixed for 5 h and then cooled to room temperature. After the precipitate was removed, CsBr (99.9%) was added, and the temperature was raised to the boiling point; the mixture was then naturally cooled to room temperature. A light

(19) Gu, Q.; Pan, Q.; Wu, X.; Shi, W.; Fang, C. *J. Cryst. Growth* **2000**, *212*, 605.
(20) Gu, Q.; Pan, Q.; Shi, W.; Sun, X.; Fang, C. *Prog. Cryst. Growth Character. Mater.* **2000**, *40*, 89.
(21) Gu, Q.; Fang, C.; Shi, W.; Wu, X.; Pan, Q. *J. Cryst. Growth* **2001**, *225*, 501.
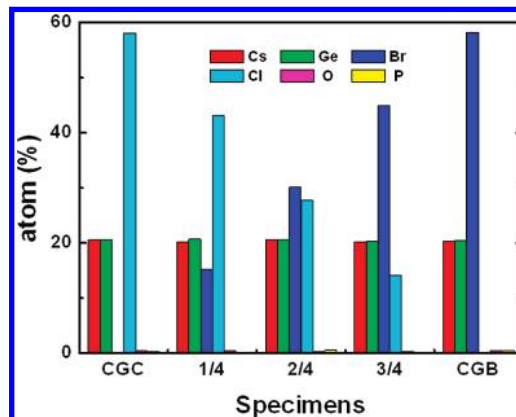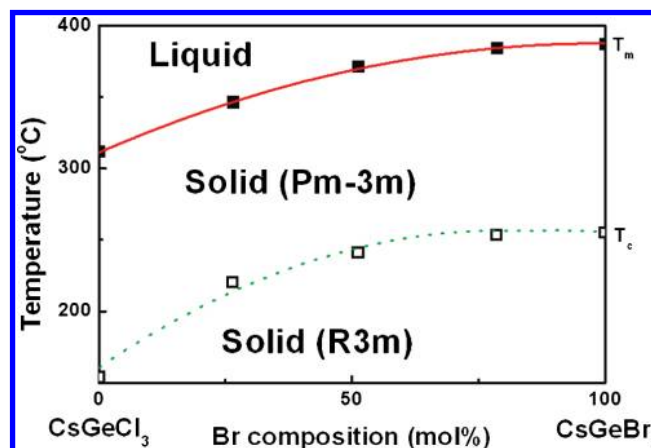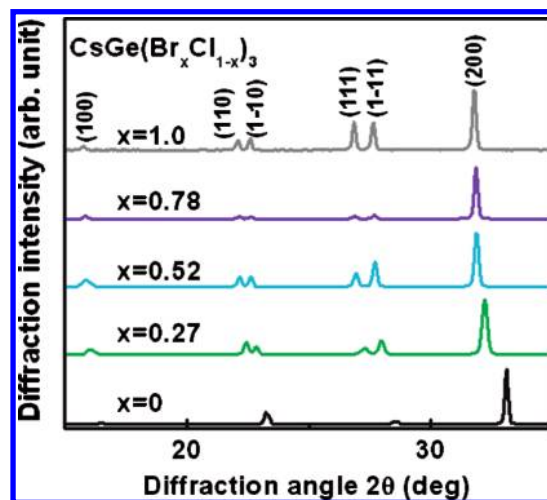(22) Christensen, A. N.; Rasmussen, S. E. *Acta Chem. Scand.* **1965**, *19*, 421.
(23) Tananaev, I. V.; Dzhurinskii, D. F.; Mikhailov, Y. N. *Zh. Neorgan. Khim.* **1964**, *9*, 1570.

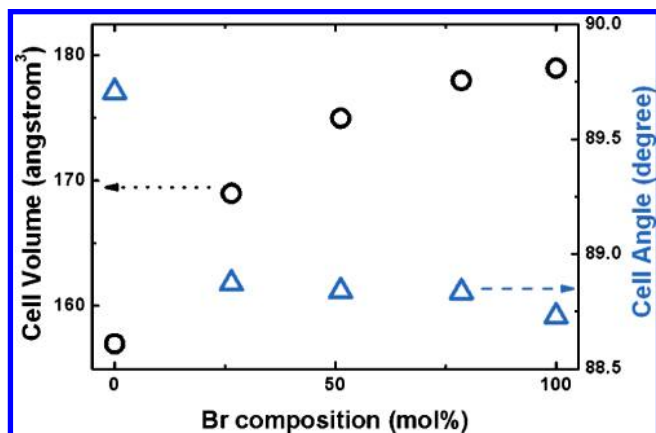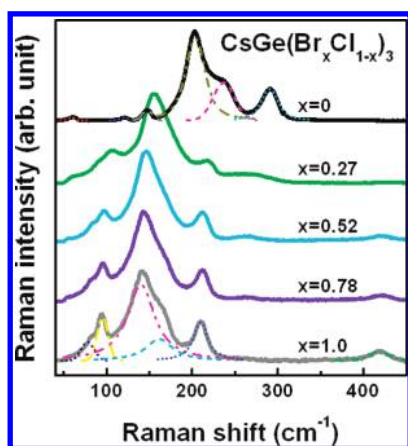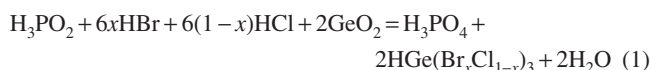**Figure 5.** The structural parameters for the NLO crystals $CsGe(Br_xCl_{1-x})_3$.

Figure 6. The Raman spectrum of $CsGe(Br_xCl_{1-x})_3$ ($R3m$) crystals at room temperature.

yellow precipitate was formed. The reaction equations were as follows.

$$H_3PO_2 + 6xHBr + 6(1-x)HCl + 2GeO_2 = H_3PO_4 +$$
$$2HGe(Br_xCl_{1-x})_3 + 2H_2O \quad (1)$$

then

$$HGe(Br_xCl_{1-x})_3 + CsCl = CsGe(Br_xCl_{1-x})_3 \downarrow + HCl \quad (2)$$

Recrystallization was performed by mixing the precipitate with 1:1 concentrated HX and alcohol solution to yield yellow crystals of $CsGe(Br_xCl_{1-x})_3$. This procedure was repeated to ensure that no residual precursor remained. Then, the crystals were dried at 85 °C for 48 h in a vacuum to prevent any effect of the deliquescence on them. The crystals were then stored at 20 °C under vacuum. However, the $CsGeBr_3$ crystal that was synthesized by Tang et al.[24] was only recrystallized once and then dried at 65 °C for 48 h in a normal atmospheric environment, so it continued to contain some impurities. The color of the precipitated product varied from yellow to white as the substitutional ratio, x, changed from 1 to 0.

2.2. Physical Measurements. The $CsGe(Br_xCl_{1-x})_3$ crystal was synthesized and sieved into particles of different sizes to measure and analyze its structural and optical properties. The crystalline structures were observed using an X-ray diffractometer. A differential scanning calorimeter (DSC) was adopted to characterize the thermal and structural behaviors of the crystals. The composition of all of the samples was measured by electron-probe X-ray

microanalysis (EPMA). Raman spectra were obtained to elucidate the atomic vibration. The optical transmission spectra in the infrared region were obtained using a Fourier-transform infrared spectrometer (FTIR). Linear optical properties were measured using an ellipsometer. The nonlinear optical properties were determined by powder second-harmonic generation measurements.

3. Results and Discussion

Figure 2 shows the composition of $CsGe(Br_xCl_{1-x})_3$ ($x = 0, 1/4, 1/2, 3/4, 1$) determined from EPMA measurements. These results reveal that these samples have a Cs to Ge ratio of almost 1:1. EPMA measurement qualitatively confirmed that chlorine atoms were successfully doped in the $CsGeBr_3$ crystal. Although it still contained some impurities, they are all smaller than 1% ($O_{max} \leq 0.47\%$, $P_{max} \leq 0.58\%$).

DSC measurements were made on polycrystalline $CsGe(Br_xCl_{1-x})_3$ in a $N_{2(g)}$ atmosphere at a heating rate of 5 °C/min to 450 °C using a Seiko SSC5000 DSC. The results, plotted in Figure 3, show that the phase-change temperatures of $CsGeCl_3$ and $CsGeBr_3$ were similar to those reported by Thiele et al.[25,26] The Curie temperature (T_c) and the melting temperature (T_m) of the $CsGe(Br_xCl_{1-x})_3$ crystals rose with Br content. The NLO $CsGe(Br_xCl_{1-x})_3$ crystals performed properly at 255.2, 253.5, 241, 220.3, and 154.1 °C for $x = 1, 3/4, 1/2, 1/4$, and 0, respectively.

XRD measurements were obtained at room temperature using Cu Kα radiation and a Siemens D5000 device to determine the structural parameters of all of the crystals $CsGe(Br_xCl_{1-x})_3$. Peak-splitting caused by the structural noncentrosymmetry, occurs mainly from $2\theta = 15°$ to $35°$. Figure 4 plots results that reveal that the substitution-related diffraction peaks shifted gradually with value of x. The measured pattern was indexed and analyzed using the program PowderCell,[27] which was developed not-for-profit by Kraus and Nolze. Some stronger diffraction peaks were observed at $2\theta = 31.76°, 27.66°, 26.86°, 22.60°, 22.10°$, and $15.76°$ from $CsGeBr_3$. These diffraction patterns were compared with JCPDS and were indexed with $(200), (1\bar{1}1), (111), (1\bar{1}0), (110)$, and (100) planes, respectively. They also confirmed that $CsGe(Br_xCl_{1-x})_3$ crystallized in the noncentrosymmetric[28] rhombohedral space group $R3m$, and the splitting differences between $(1\bar{1}1)$ with (111) and between $(1\bar{1}0)$ with (110) become closer as the Br content in $CsGe(Br_xCl_{1-x})_3$ decreases. The cell parameters, which were extracted from the powder-XRD in Figure 5 indicated that the cell volume increased with Br content while the cell angle decreased. Therefore, the structural distortion of $CsGe(Br_xCl_{1-x})_3$ ($R3m$) increased with Br.

In the Raman scattering measurement, the $CsGe(Br_xCl_{1-x})_3$ samples were illuminated at room temperature using an argon ion laser at 488 nm with an average power of 30 mW. Figure 6 plots the results. The Raman peaks shift with the Br

(24) Tang, L. C.; Huang, J. Y.; Chang, C. S.; Lee, M. H.; Liu, L. Q. *J. Phys.: Condens. Matter* **2005**, *17*, 7275.

(25) Thiele, G.; Rotter, H. W.; Schmidt, K. D. *Z. Anorg. Allg. Chem.* **1987**, *545*, 148.
(26) Thiele, G.; Rotter, H. W.; Schmidt, K. D. *Z. Anorg. Allg. Chem.* **1988**, *559*, 7.
(27) Kraus, W.; Nolze, G. *J. Appl. Crystallogr.* **1996**, *29*, 301.
(28) Seo, D. K.; Gupta, N.; Whangbo, M. H.; Hillebrecht, H.; Thiele, G. *Inorg. Chem.* **1998**, *37*, 407.

Table 1. The Raman Spectra Comparison for the Ternary Halides CsGe(Br$_x$Cl$_{1-x}$)$_3$[a]

symmetry	overtone			A$_1$	E	A$_1$		overtone
specimens	w	m	s	vs	ls	s	w	w
$x = 1.00$	49	77	91	139	160	210		refs 18 and 25
$x = 1.00$	50.50	78.50	93.99	140.31	159.88	209.79		419.21
$x = 0.78$	52.32	82.97	94.78	142.66	163.00	211.25	264.10	421.27
$x = 0.52$	53.94	84.18	95.57	144.23	163.78	212.90	264.10	421.50
$x = 0.27$	55.08	91.27	103.43	152.84		212.58	268.48	423.37

symmetry	m	w	m	A$_1$	E	A$_1$	
				vs	ls	s	
$x = 0.00$	58.50	121.49	146.58	202.79	236.98	291.15	
$x = 0.00$	57	120	145	200	237	290	refs 18 and 25

[a] The descriptions of the peaks are vs = very strong, s = strong, ls = less strong, m = middle, and w = weak. The unit of these Raman peaks was cm^{-1}.
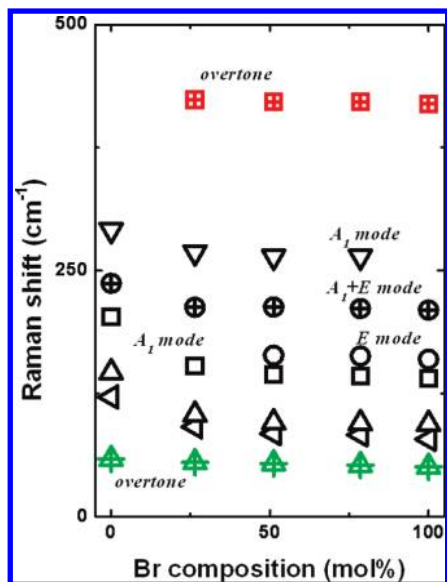

Figure 7. Raman vibrational modes of CsGe(Br$_x$Cl$_{1-x}$)$_3$ ($R3m$) crystals at room temperature.

Table 2. The Ellipsometry Measurements of the Rhombohedral NLO Crystals CsGe(Br$_x$Cl$_{1-x}$)$_3$ (x = 0, 1/4, 1/2, 3/4, 1)

CsGe(Br$_x$Cl$_{1-x}$)$_3$	$x = 0.00$	$x = 0.27$	$x = 0.52$	$x = 0.78$	$x = 1.00$
α_{630nm} (1/mm)	1.49	3.80	5.26	4.45	8.88
n_{630nm}	1.71	1.89	1.78	1.58	1.63
n_{1260nm}	1.67	1.86	1.78	1.64	1.68

content, which is consistent with the fact that the phonon frequency is inversely proportional to the square root of the mass of GeX$_3$ (X = Cl, Br). The data agree closely with the Raman spectra of CGC and CGB;[25,18] Table 1 summarizes the results. The strongest Raman peaks "vs" (column 4) of the CsGe(Br$_x$Cl$_{1-x}$)$_3$ crystals are attributable to the A$_1$ mode. Raman peaks from 264 to 292 cm^{-1} (column 7) are also associated with the A$_1$ mode. Another group of Raman peaks (from 159 to 164 cm^{-1}, column 5) can be attributed to the E mode. The other group of Raman peaks (from 209 to 237 cm^{-1}, column 6) is attributable to the A$_1$ + E mode. Raman peaks of CGB occuring at 419.21 and 209.79 cm^{-1} can be assigned to the corresponding (50.5 cm^{-1}) overtones. The Raman peaks of CGC at 236.98 cm^{-1} are assigned to the corresponding (58.5 cm^{-1}) overtone. Therefore, columns 6 and 8 are assigned to the corresponding (column 1) overtones (Figure 7). Figure 7 and Table 1 reveal that columns 2–5 and 7 are related to the anion substitution. Column 5 relates to the bromine atom while column 7 relates only to the
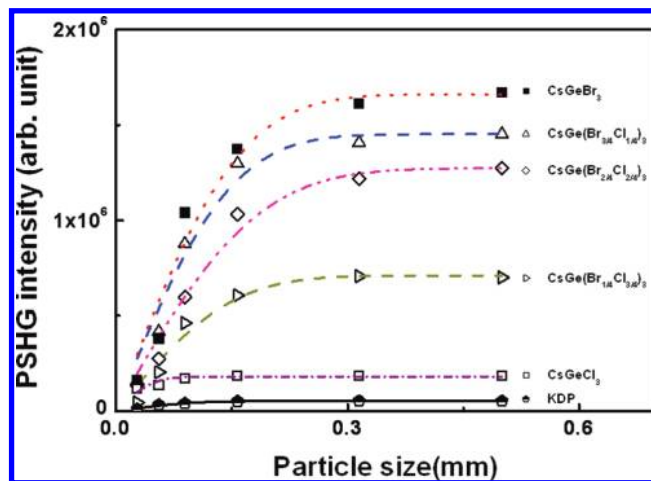
Figure 8. The comparison of integrated powder second-harmonic generation intensity of nonlinear optical crystals of KDP and CsGe(Br$_x$Cl$_{1-x}$)$_3$.
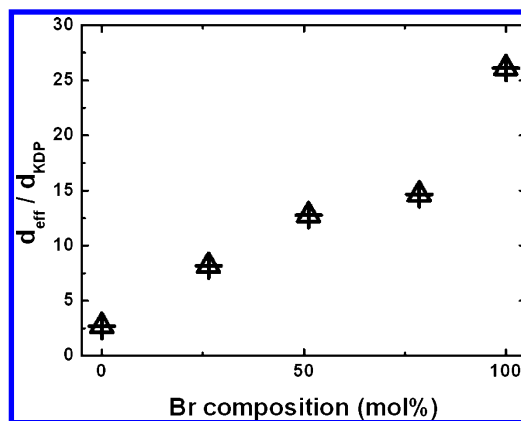
Figure 9. The effective powder second-harmonic generation coefficients of nonlinear optical crystals CsGe(Br$_x$Cl$_{1-x}$)$_3$.

chlorine atom. Columns 2–4 relate to the bonds of Ge–X$_3$. This result is consistent with the effective-mass concept, on which basis the oscillation frequency is expected to increase as Br content decreases, since the Br atom is heavier than Cl. Columns 1, 6, and 8 are associated with the oscillations between Cs$^+$ and Ge(Br$_x$Cl$_{1-x}$)$_3^{-1}$ because they are less influenced by the anion substitution.

Powder SHG measurements were made using a modified Kurtz-NLO[29] system using light of wavelength 1260 nm. When the SHG process was phase-matchable and satisfied

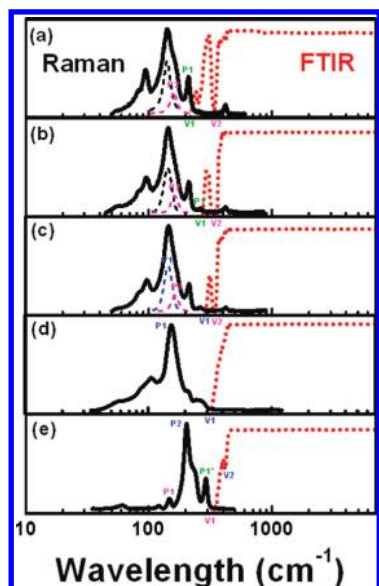(29) Kurtz, S. K.; Perry, T. T. *J. Appl. Phys.* **1968**, *39*, 3798.

Figure 10. Raman scattering versus IR absorption spectra of CsGe ($Br_xCl_{1−x}$)$_3$: (a) $x = 1.00$; (b) $x = 0.78$; (c) $x = 0.52$; (d) $x = 0.27$; (e) $x = 0.00$.

Table 3. The IR Absorption/Raman Spectra of CsGe($Br_xCl_{1−x}$)$_3$[a]

specimens	P_1	P_2	P_1'	V_1	V_2
$x = 1.00$	209.79	159.88		212.14	333.25
$x = 0.78$	264.10	163.00		269.64	330.94
$x = 0.52$	144.23	163.78		281.57	332.48
$x = 0.27$	152.84			311.65	
$x = 0.00$	146.58	202.79	291.15	305.48	414.25

[a] The units for these Raman and FTIR peaks were cm^{-1}. P = Raman peak; V = FTIR valley.
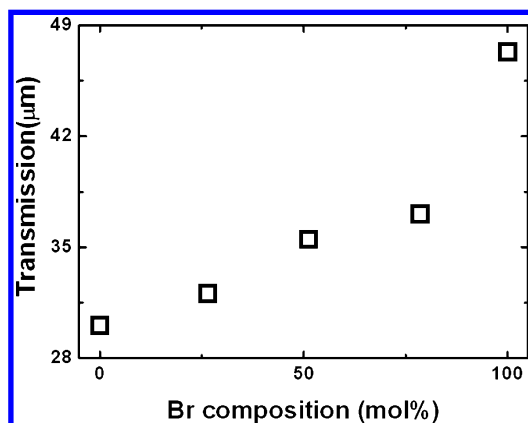

Figure 11. The transmission edge (limited by the phonon absorption of the crystals) of CsGe($Br_xCl_{1−x}$)$_3$ crystals.

the type-I phase-matching conditions, the intensity of the SHG response was given by[30]

$$I_{2\omega}(\bar{r}, \theta) = \frac{128\pi^5 I_\omega^2}{n_\omega^2 n_{2\omega} \lambda_{2\omega}^2 c} L\bar{r}\langle d_{eff}^2\rangle \frac{\left[\sin^2\frac{\pi}{2}\frac{\bar{r}}{\bar{l}_{pm}}(\theta - \theta_{pm})\right]}{\left[\frac{\pi}{2}\frac{\bar{r}}{\bar{l}_{pm}}(\theta - \theta_{pm})\right]} \quad (3)$$

where $\bar{l}_{pm} = \lambda/(4|\Delta n_{B,2\omega}|\sin 2\theta_{pm})$, and θ_{pm} is the phase-matching angle. Here $\Delta n_{B,2\omega} = n_{E,2\omega} - n_{0,2\omega}$ denotes the birefringence of the material at the second-harmonic wave-

(30) Prasad, P. N.; Williams, D. J. *Introduction to Nonlinear Optical Effects in Molecules and Polymers*; Wiley: New York, 1991; Chapter 6.
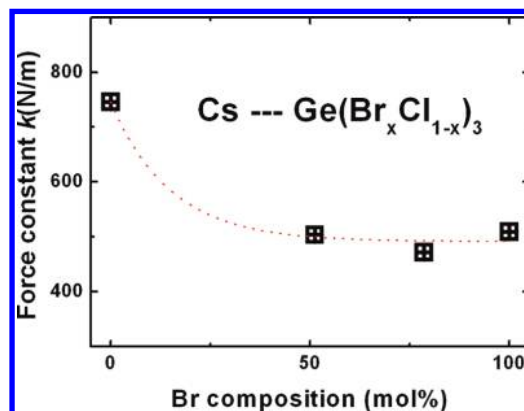
Figure 12. The force constants of bonds between Cs^+ and anion group Ge($Br_xCl_{1−x}$)$_3^{-1}$ of CsGe($Br_xCl_{1−x}$)$_3$ crystals.

length. In the event that $\bar{r} \gg \bar{l}_{pm}$ or $\bar{r} \ll \bar{l}_{pm}$, eq 3 can be simplified to

$$I_{2\omega} \rightarrow \begin{cases} [(256\pi^4 I_\omega^2)/(n_\omega^2 n_{2\omega}\lambda_{2\omega}^2 c)]L\bar{l}_{pm}\langle d_{eff}^2\rangle, \leftarrow \bar{r} \gg \bar{l}_{pm} \\ [(128\pi^5 I_\omega^2)/(n_\omega^2 n_{2\omega}\lambda_{2\omega}^2 c)]L\bar{r}\langle d_{eff}^2\rangle, \leftarrow \bar{r} \ll \bar{l}_{pm} \end{cases}$$
(4)

The SHG signals became saturated when the average particle sizes were larger than $\bar{l}_{pm}$ and were independent of the particle size.

Chen et al.[31] derived a useful empirical formula, which had the correct asymptotic forms of eq 4, to elucidate the overall variation in the second harmonic $\bar{r}$

$$I_{2\omega} = \frac{256\pi^4 I_\omega^2}{n_\omega^2 n_{2\omega}\lambda_{2\omega}^2 c} L\bar{l}_{pm}\langle d_{eff}^2\rangle\sqrt{1 - \exp[-(\bar{r}/A)^2]} \quad (5)$$

with $A \approx 9\bar{l}_{pm}$.

The saturated PSHG intensity decayed because the absorption coefficient of CsGeBr$_3$ at 630nm was too large. The absorption coefficients (from Table 2) were adopted to calculate the real saturated PSHG intensity using $I_{2\omega} = I_{2\omega}^{total} e^{-\alpha z}$ to modify the situation. The square of the effective nonlinearity, $\langle d_{eff}^2\rangle$, averaged over the orientation distribution of crystalline powders of CsGe($Br_xCl_{1−x}$)$_3$ was determined by eq 6 using a reference NLO crystal, such as KDP.

$$\langle d_{eff}^2\rangle_{CGBC} = \langle d_{eff}^2\rangle_{KDP} \frac{I_{2\omega,CGBC}^{total} n_{\omega,CGBC}^2 n_{2\omega,CGBC}}{I_{2\omega,KDP}^{total} n_{\omega,KDP}^2 n_{2\omega,KDP}}$$

$$\approx \langle d_{eff}^2\rangle_{KDP} \frac{I_{2\omega,CGBC}^{total} n_{CGBC}^3}{I_{2\omega,KDP}^{total} n_{KDP}^3} \quad (6)$$

when $n \approx n_\omega \approx n_{2\omega}$.

The results, plotted in Figure 8, revealed that the SHG efficiencies of CsGe($Br_xCl_{1−x}$)$_3$ were higher than that of KDP. All were phase-matchable as was KDP, meaning that as the particle size becomes substantially larger than the coherence length of the crystal, the collected SHG intensity does not gain anymore but saturates at a certain value. The saturated PSHG intensities were estimated from the transmission signals from particles of various sizes and demonstrated that the SHG responses became stronger as the Br content

increased. The d_{eff}/d_{KDP} values were calculated from Table 2 and are shown in Figure 9. The effective powder second-harmonic generation coefficients increased with Br content. CGB was about 9.64 times that of CGC and 28.29 times that of KH$_2$PO$_4$ (KDP). The structural distortion and the off-center Ge ion in the unit cell contributed to the SHG responses. The results of XRD demonstrate that the structural distortion increased with Br content. The cell angle distortion also increased with Br content. Hence, the position of the B-site cation, Ge, becomes closer to the cell corner as Br content increases.

Infrared spectra were obtained using a spectrometer (Bomem, DA8.3) in the range from 120 to 4000 cm^{-1} as the specimens were pressed into thin plates ($\sim$500 μm). Figure 10 and Table 3 reveal that the actual IR transparency edges in the vibrational IR absorption/Raman spectra of CsGe(Br$_x$Cl$_{1-x}$)$_3$ are V1 and P1, which can be associated with two-phonon absorption for $x = 0$ to 1/2. The further absorption V2 is related to two-phonon absorption that involves the next vibrational band P2.

Figure 10 plots FTIR measurements that demonstrate that the long wavelength limit of the transparent range of the crystals similarly depends on the amount of substitution (Figure 11). Crystal CsGeCl$_3$ had an infrared cutoff wavelength at $\sim$30 μm, which was shorter than the cutoff value of CsGeBr$_3$ ($\sim$47 μm). The infrared absorption edge of CsGe(Br$_x$Cl$_{1-x}$)$_3$ with $x = 1/4$, 1/2, or 3/4 lie approximately from 32 to 37 μm. This result agrees with the effective-mass concept based on which the infrared transparency range of CGB is expected to be wider than that of CGC because the Br atom is heavier than Cl.

The force constants between the Cs$^+$ and Ge(Br$_x$Cl$_{1-x}$)$_3^{-1}$ oscillations are calculated from the FTIR peaks (Figure 10) in the range 290 to 410 cm^{-1} according to $\omega = 1/(2\pi c)(k/u)^{1/2} = 5.3 \times 10^{-12}(k/u)^{1/2}$,[32] where ω is the wavenumber of an absorption peak in cm^{-1}, k is the force constant of the bond in newtons per meter (N/m), c is the velocity of light in cm/s, and μ is the reduced mass in kg. The force constant increases as Br content declines (Figure 12), indicating that the oscillation frequency increases as the Br content falls. The result is also consistent with the trend of A$_1$ + E mode (which refers to the oscillation between Cs$^+$ and Ge(Br$_x$Cl$_{1-x}$)$_3^{-1}$ of the Raman spectrum (Figure 7).

4. Conclusions

Based on the experimental results of CsGe(Br$_x$Cl$_{1-x}$)$_3$ ($x = 0$, 1/4, 1/2, 3/4, and 1), the linearly increasing x increases Curie temperature, cell volume, second-order NLO susceptibility, and transparency range but reduces the cell angle and the force constant. Therefore, the properties of CsGe(Br$_x$Cl$_{1-x}$)$_3$ crystals could be modulated by anion substitution.

(31) Chen, W. K.; Cheng, C. M.; Huang, J. Y.; Hsieh, W. F.; Tseng, T. Y. *J. Phys. Chem. Solids* **2000**, *61*, 969.
(32) Skoog, D. A.; Leary, J. J. *Principles of Instrumental Analysis*; Academic Press: New York, 1992.